Available online at www.sciencedirect.com

ScienceDirect

Energy Procedia 55 (2014) 750 – 756

Energy Procedia

4th International Conference on Silicon Photovoltaics, SiliconPV 2014

The influence of orientation and morphology on the passivation of crystalline silicon surfaces by Al_2O_3

Lachlan E. Black[a,*], Teng C. Kho[a], Keith R. McIntosh[b], and Andres Cuevas[a]

[a]*Research School of Engineering, The Australian National University, Canberra, ACT 0200, Australia*
[b]*PV Lighthouse, Coledale, NSW 2515, Australia*

Abstract

We compare the passivation provided by Al_2O_3 deposited on planar <100> and <111>, and textured <100>, boron-diffused and undiffused crystalline silicon surfaces. The passivation of <111> surfaces is found to be somewhat worse than that of <100> surfaces for the as-deposited films, but improves to similar values after annealing. Higher recombination at textured surfaces compared to planar <111> surfaces can be largely, though not entirely, attributed to the difference in surface area. The passivation of both as-deposited and annealed films is found to improve over time when stored under ambient conditions. This helps give context to the myriad of results reported on planar <100> samples – we expect J_0 values measured for Al_2O_3 layers on such surfaces to increase by a factor of ~2 to 3 on textured surfaces.

Peer-review under responsibility of the scientific committee of the SiliconPV 2014 conference

Keywords: silicon; surface passivation; aluminium oxide

1. Context and previous work

Thin film amorphous aluminium oxide (Al_2O_3) has received a great deal of attention from the photovoltaic community in recent years due to its outstanding surface passivation properties when applied to crystalline silicon (c-Si) surfaces [1–7]. Its low interface defect density and large negative charge allow it to provide unsurpassed passivation of *p*-type c-Si surfaces, to the extent that measurements of Al_2O_3-passivated samples have necessitated a re-evaluation of the intrinsic limits to the bulk carrier lifetime of silicon [8]. It is therefore a prime candidate both to

* Corresponding author. *E-mail address:* lachlan.black@anu.edu.au

Peer-review under responsibility of the scientific committee of the SiliconPV 2014 conference
doi:10.1016/j.egypro.2014.08.055

replace the Al-BSF for rear side passivation in conventional p-type cells, and to provide passivation for the boron-doped *p*+ region in new high-efficiency *n*-type cell structures.

In both of these applications, Al_2O_3 passivation layers are likely to be applied to surfaces that are far from planar. Particularly for *p*+ regions, which are typically located on the front surface of the cell, some surface structure, usually a random pyramid texture, is mandated by the need for effective light-trapping. However, even on the rear of the cell, the use of a textured surface can have optical benefits while reducing process complexity. It is well known that the presence of such a texture can exert a significant influence on the quality of a dielectric passivation, both through increased surface area, the exposure of <111> oriented crystalline facets, and potentially via other mechanisms such as the influence of mechanical stress at the edges and vertices of surface features [9]. Previous studies of the influence of such factors for other dielectrics such as SiO_2 and SiN_x have revealed differences of up to five-fold in the passivation quality between <100> and <111> orientations, and even greater differences between planar and textured surfaces [9].

It is somewhat surprising, therefore, that relatively little systematic work has been performed to assess the impact of either crystalline orientation or surface morphology on the passivation performance of Al_2O_3. The great majority of reported passivation data are for planar <100> surfaces, and although some scattered results on <111> surfaces have been reported, there has generally been no effort to compare these directly to results on <100> surfaces. An exception is the recent work of [10], which examined the surface passivation of Al_2O_3 from atomic layer deposition (ALD), both thermal and plasma-assisted, on diffused and undiffused planar surfaces of <100> and <111> orientation, finding generally slightly worse passivation properties for <111> surfaces. However, no comparison to textured surfaces was made in that work.

Numerous examples of the application of Al_2O_3 to textured surfaces within device structures exist in the literature, but again there are relatively few direct comparisons to planar surfaces. Duttagupta et al. [11] measured the passivation quality of plasma-enhanced chemical vapour deposition (PECVD) Al_2O_3/SiN_x stacks on boron-diffused textured and planar <100> samples, reporting a textured-to-planar J_0 ratio of 1.5–2. A similar experiment was performed by [12] with both Al_2O_3/SiN_x stacks and Al_2O_3 by itself, where the Al_2O_3 was deposited by plasma-assisted ALD. They reported a textured-to-planar J_0 ratio between 1.7 and 2.5. However, neither [11] nor [12] included a comparison to planar <111> surfaces, which leaves the role played by the <111> surface orientation of the textured surface open to speculation.

In this work, we perform measurements of surface passivation quality for Al_2O_3–passivated boron-diffused and undiffused surfaces, both planar <100>, planar <111>, and with a random pyramid texture. This allows us to separate the influence of crystal orientation and surface area from any additional effects, on differences in the recombination rate between planar and textured silicon surfaces.

2. Experimental procedure

Boron-diffused symmetrical lifetime structures were prepared on high resistivity (>100 Ω·cm) *n*-type <100> and <111> float-zone silicon wafers, approximately 450 and 325 μm thick respectively. The latter were supplied with a chemical polish by the manufacturer, and were used without additional etching, while the former received either a planar etch in $HF:HNO_3$ or TMAH solution, or a random pyramid texture in TMAH. All samples received an initial boron diffusion of ~110–120 Ω/□, with some receiving additional drive-in anneals of 1, 3, or 6 hours at 1100 °C in N_2 in order to vary the surface dopant concentration and diffusion profile. Additional undiffused samples were prepared on various substrates (details in Table 1) in the same way. All samples were given an RCA clean and HF dip prior to Al_2O_3 deposition.

The Al_2O_3 films were deposited by atmospheric pressure chemical vapour deposition (APCVD) using an inline APCVD belt furnace tool developed by Schmid Thermal Systems [6, 13]. Triethyldialuminium-tri-(*sec*-butoxide) (TEDA-TSB) and H_2O were used as precursors, with a substrate temperature of ~440°C. The films were deposited sequentially on the front and the rear of the samples. Characterisation was performed both before and after annealing in a quartz tube furnace at 425°C in N_2 for 30 minutes.

Measurements of the effective excess carrier lifetime τ_{eff} vs excess carrier concentration Δn were performed using a Sinton Instruments WCT-120 photoconductance tool, generally under quasi-steady-state (QSS) illumination conditions. The optical constant required to determine the generation rate was determined by comparison of QSS

measurements with those performed under transient illumination conditions, over the range of Δn in which both methods were valid, or by comparison with the transient lifetime tail present in the QSS measurement itself following the illumination cutoff. Values of the optical constant determined in this way ranged from 0.59 to 0.64 for the planar samples, with values of 0.80 and 0.90 for the undiffused and diffused textured samples respectively.

3. J_0 extraction

The recombination rate at both diffused and undiffused surfaces was characterised in terms of the saturation current density J_0, calculated according to:

$$J_0 = \frac{qWn_i^2}{2}\frac{d}{d\Delta n}\left(\frac{1}{\tau_{eff}} - \frac{1}{\tau_{bulk,intrinsic}}\right) \quad (1)$$

where q is the fundamental charge, W is the wafer thickness, $n_i = 9.7 \times 10^9$ cm^{-3} is the intrinsic carrier concentration in silicon, calculated using the expression of [14] at 300 K, and $\tau_{bulk,intrinsic}$ is the Auger-limited intrinsic bulk lifetime, calculated using the empirical parameterization of [8].

Fig. 1 shows the J_0 extraction from the Auger-corrected inverse lifetime for the undiffused samples. In most cases J_0 was determined from the slope of the data around $\Delta n = 1.8\times10^{16}$ cm^{-3}. For the as-deposited textured sample, only a transient photoconductance measurement was performed immediately after deposition, which results in an apparent reduction in inverse lifetime at higher Δn due to non-zero generation. Therefore for this sample the slope was extracted at $\Delta n = 5\times10^{15}$ cm^{-3}, and it was confirmed that this resulted in agreement with measurements at higher Δn for the same sample when later remeasured using both transient and QSS illumination. Note that for the more lightly doped <111> samples τ_{eff}^{-1} is artificially reduced at lower Δn due to depletion region modulation. The resulting J_0 values are given in Table 1.

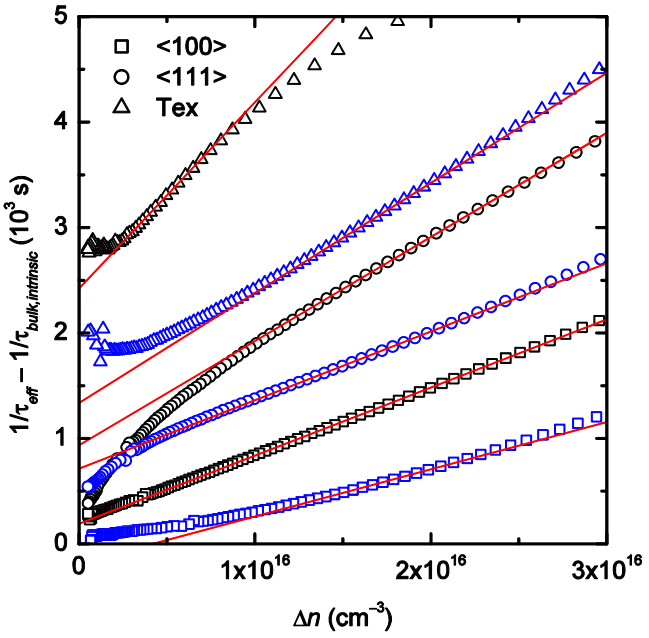

Fig. 1. Auger-corrected inverse effective lifetime for the undiffused n-type samples. Lines show the linear fits used to extract J_0.

Table 1. Parameters of the undiffused *n*-type samples.

Surface	Finish	Resistivity (Ω·cm)	Dopant Concentration (cm^{-3})	Thickness (μm)	J_0 as-deposited (fA cm^{-3})	J_0 annealed (fA cm^{-3})
Planar <100>	polished	1.5	3×10^{15}	235	11.4	7.9
Planar <111>	HF:HNO_3	15	3×10^{14}	223	16.6	10.9
Textured	TMAH	2.3	2×10^{15}	234	31.1	18.4

For the diffused samples, accurate extraction of J_0 is somewhat more complicated. Equation (1) is based on the assumption that Δn is spatially uniform throughout the thickness of the sample (ie, Δn is the same at the surfaces and everywhere in the bulk of the wafer). This assumption is practically necessary, since only the average carrier concentration, Δn_{av}, is generally accessible to experiment. However, it is never strictly true, even for spatially uniform carrier generation, because surface recombination is always non-zero, and carrier mobilities are finite [15]. When surface recombination is significant, Δn becomes significantly non-uniform due to the limited diffusion rate of carriers from the bulk to the surfaces, such that Δn_{av} is significantly greater than Δn at the surfaces. Since the lifetime of carriers at the surface decreases with increasing Δn in high injection, this leads to an increasing overestimation of Δn at the surfaces with increasing Δn_{av}, and a consequent underestimation of the apparent J_0 determined by (1). This will occur even for samples with low J_0 in sufficiently high injection, and the error will become significant at lower Δn as J_0 increases. Conversely, since $\tau_{bulk,intrinsic}$ in (1) is calculated from Δn_{av}, and has approximately an inverse quadratic dependence on Δn, this value will be increasingly and systematically overestimated, which will tend to increase the apparent J_0, especially as Auger recombination begins to dominate at very high Δn.

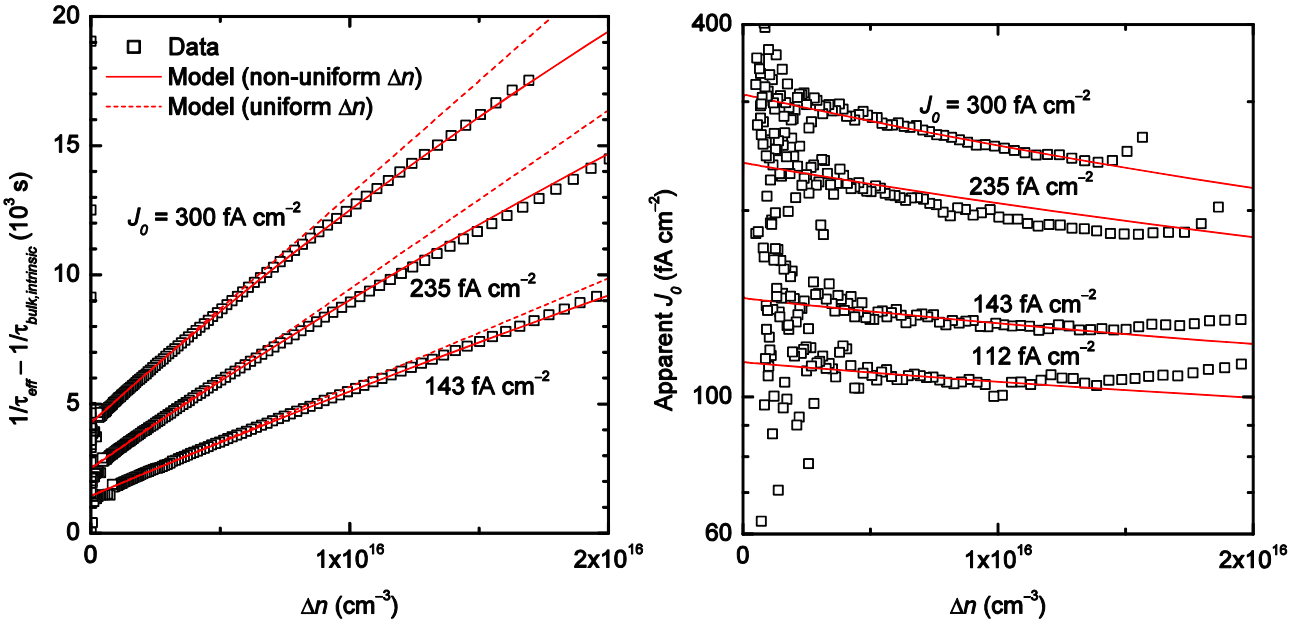

Fig. 2. (a) Auger-corrected inverse effective lifetime for selected boron-diffused and textured samples, showing the Δn-dependent slope resulting from non-uniformities in the carrier profile at high J_0; (b) apparent J_0 determined from (1) vs Δn for the same samples. Solid lines show the dependence predicted by numerical modeling due to nonuniformity in the excess carrier profile, while dashed lines show the dependence predicted under the assumption of a uniform carrier profile.

Fig. 2 shows that these predicted experimental dependencies of the apparent J_0 on Δn do in fact manifest in practice for the samples of this study, in good agreement with numerical simulations performed using the model described in [16]. The consequence is that the conventional practice of extracting J_0 for $\Delta n = 10^{16}$ cm^{-3} or above will

result in significant underestimation for samples with higher J_0, such as those with a textured diffused surface. This is obviously a problem if we wish to compare samples with dissimilar values of J_0. For some samples, primarily those with planar <111> and (in some cases) textured surfaces and as-deposited Al_2O_3 layers, the dependence of the apparent J_0 on Δn was found to be even stronger than that predicted by modeling. It may be that in these samples additional mechanisms are present, for example lateral spatial non-uniformity of the surface passivation itself. This enhanced dependency is no longer seen for the same samples after annealing, which suggests that it is indeed most likely related to the properties of the passivation layer.

Given these additional factors, the extraction of J_0 by comparison to numerical modelling is not straightforward. However, it is clear that, as shown in Fig. 2, the error in J_0 is minimized by performing the extraction at lower values of Δn. Consequently, for these samples we chose to determine J_0 by applying (1) to the data measured at lower Δn, generally within the range $1.5\times10^{15} < \Delta n < 4\times10^{15}$ cm^{-3}.

4. Results and discussion

Fig. 3 shows J_0 values measured on diffused surfaces for the Al_2O_3 films as-deposited and after annealing. Measurements of the as-deposited films were performed both immediately after deposition and immediately before annealing, approximately 18 hours later. It was found that the surface passivation of all samples, particularly the textured samples, improved significantly over this time under ambient conditions. A similar effect was observed for the annealed samples when remeasured 24 days after annealing. No significant difference in J_0 between planar <100> surfaces prepared by HF:HNO_3 and TMAH etches was observed.

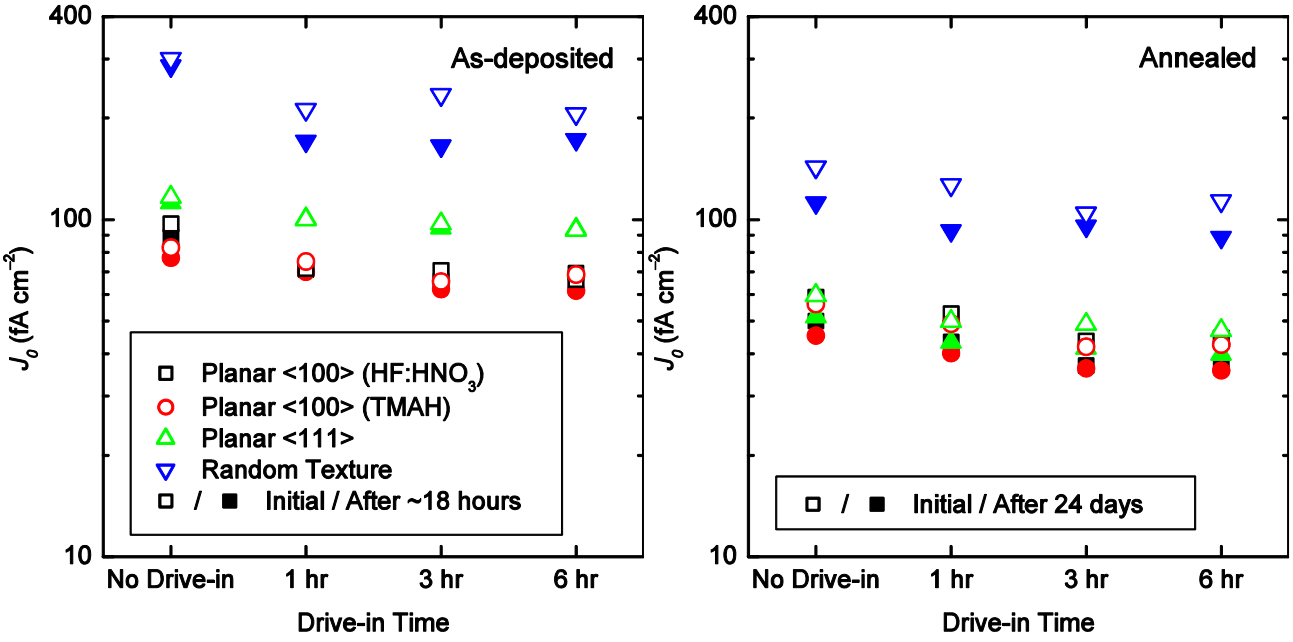

Fig. 3. J_0 of the boron-diffused planar <100>, planar <111>, and random textured samples with (a) as-deposited, and (b) annealed Al_2O_3 layers. Values are shown as measured immediately after deposition, immediately before annealing (~18 hours later), immediately after annealing, and 24 days after annealing.

The ratio of J_0 for planar <111> surfaces relative to planar <100> (Fig. 4a) was generally in the range of 1.3–1.5 for the as-deposited films on both diffused and undiffused surfaces, decreasing to 1–1.2 after annealing for the diffused surfaces. This suggests either a higher interface defect density or lower fixed charge for the <111> interface compared to <100>, as well as a relative improvement in one or both properties following annealing. The ratio for undiffused surfaces was similar to that of diffused surfaces for the as-deposited films, but did not change

significantly after annealing. The reason for this difference is not clear. We note that while Auger recombination in the diffused region also contributes to J_0, and should be independent of surface orientation, its contribution is expected to be small relative to surface recombination for such lightly diffused surfaces.

The ratio of J_0 for textured surfaces relative to planar <111> (Fig. 4b) was found to be between 2.2 and 2.6 for most of the diffused samples. Since this value is higher than the geometric surface area ratio of 1.73 (or possibly 1.66 [17]), this implies the existence of an additional recombination enhancement factor due to the surface structure. A notable exception is the data for the unannealed films measured ~18 hours after deposition, where the J_0 ratio is very close to the geometric ratio. One tentative hypothesis might be that these unannealed films contain significantly more hydrogen, which allows for a greater degree of lattice relaxation in the vicinity of abrupt surface features, and hence less strain and consequent creation of unsatisfied ("dangling") bonds. In contrast, J_0 ratios for the undiffused surfaces were found to be quite close to the geometric ratio, so that for these samples the increase in J_0 for textured surfaces over planar <111> can be explained solely by the difference in surface area.

The results presented in Fig. 4 are in broad agreement with the previous work of [11] and [12]. Their ranges of 1.5 to 2.0, and 1.7 to 2.5 for the ratio of J_0 at textured and planar <100> surfaces may be compared with the range of 2.0 to 3.3 measured here. The relatively limited influence of orientation and surface structure on recombination at Al_2O_3-passivated Si surfaces is in marked contrast to the case for SiO_2 and SiN_x. This points to fundamental differences in the structure of the Si–Al_2O_3 interface with respect to that of these other dielectrics.

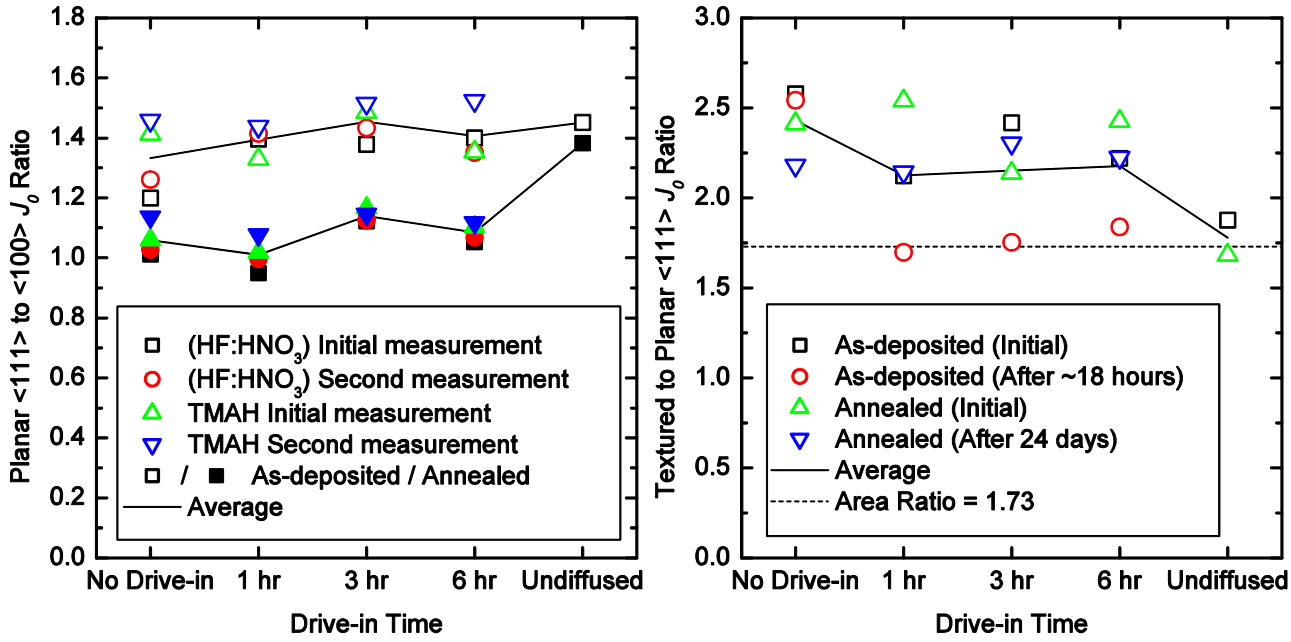

Fig. 4. Ratio of J_0 for (a) planar <111> to planar <100> surfaces, and (b) textured to planar <111> surfaces. Data is shown for both boron-diffused surfaces and undiffused *n*-type surfaces. Values are shown as measured immediately after deposition, immediately before annealing (~18 hours later), immediately after annealing, and 24 days after annealing.

5. Conclusion

We have shown that the increase in J_0 at undiffused, randomly textured silicon surfaces passivated by Al_2O_3, with respect to planar <100> surfaces, may be entirely attributed to 1) the <111> surface orientation of the pyramid facets and 2) the increased surface area. For boron-diffused surfaces an additional factor due to surface features *may* be present, but is relatively small, in the range of 1.0 to 1.5. The increase of J_0 at <111> surfaces relative to <100> is also small, though the precise value will depend on the particular Al_2O_3 layer in question. In general one can expect J_0 values measured for Al_2O_3 on <100> Si surfaces to increase by a factor of ~2 to 3 when the same films are applied

to textured surfaces. The relatively limited dependence of Si–Al_2O_3 interface recombination on orientation and surface structure is in marked contrast to the case for SiO_2 and SiN_x, and makes Al_2O_3 a particularly attractive candidate to passivate non-planar surfaces.

References

[1] Agostinelli G, Delabie A, Vitanov P, Alexieva Z, Dekkers HFW, De Wolf S, Beaucarne G, Very low surface recombination velocities on p-type silicon wafers passivated with a dielectric with fixed negative charge, Sol Energy Mater Sol Cells 2006;90:3438.
[2] Hoex B, Heil SBS, Langereis E, van de Sanden MCM, Kessels WMM, Ultralow surface recombination of c-Si substrates passivated by plasma-assisted atomic layer deposited Al_2O_3, Appl Phys Lett 2006;89:042112-1–042112-2.
[3] Li TT, Cuevas A, Effective surface passivation of crystalline silicon by rf sputtered aluminum oxide, Phys Status Solidi: RRL 2009;3:160.
[4] Saint-Cast P, Kania, D, Hofmann M, Benick J, Rentsch J, Preu R, Very low surface recombination velocity on p-type c-Si by high-rate plasma-deposited aluminum oxide, Appl Phys Lett 2009;95:151502-1–151502-3.
[5] Miyajima S, Irikawa J, Yamada A, Konagai M, High quality aluminum oxide passivation layer for crystalline silicon solar cells deposited by parallel-plate plasma-enhanced chemical vapor deposition, Appl Phys Express 2010;3:012301-1–012301-3.
[6] Black LE, McIntosh KR, Surface passivation of c-Si by atmospheric pressure chemical vapour deposition of Al_2O_3, Appl Phys Lett 2012;100:202107-1–202107-5.
[7] Zhang X, Cuevas A, Thomson A, Annealing of Al_2O_3 thin films prepared by atomic layer deposition, IEEE J Photovoltaics 2013;3:183.
[8] Richter A, Glunz SW, Werner F, Schmidt J, Cuevas A, Improved quantitative description of Auger recombination in crystalline silicon, Phys Rev B 2012;86:165202-1–14.
[9] Baker-Finch SC, McIntosh KR, The contribution of planes, vertices, and edges to recombination at pyramidally textured surfaces, IEEE J Photovoltaics 2011;1:59–65.
[10] Liang WS, Weber KJ, Suh D, Phang SP, Yu J, McAuley AK, Legg BR, Surface passivation of boron-diffused p-type silicon surfaces with (100) and (111) orientations by ALD Al_2O_3 layers, IEEE J Photovoltaics 2013;3:678–683.
[11] Duttagupta S, Lin F, Shetty KD, Aberle AG, Hoex B, Excellent boron emitter passivation for high-efficiency Si wafer solar cells using AlO_x/SiN_x dielectric stacks deposited in an industrial inline plasma reactor, Prog Photovoltaics: Res Appl 2012;21;760–764.
[12] Richter A, Benick J, Hermle M, Boron emitter passivation with Al_2O_3 and Al_2O_3/SiN_x stacks using ALD Al_2O_3, IEEE J Photovoltaics 2013;3:236–245.
[13] Black LE, Provancha KM, McIntosh KR, Surface passivation of crystalline silicon by APCVD aluminium oxide, Proceedings 26th EUPVSEC, Hamburg, Germany, 2011. pp. 1120-1124.
[14] Misiakos K, Tsamakis D, Accurate measurements of the silicon intrinsic carrier density from 78 to 340 K, J Appl Phys 1993;74:3293–3297.
[15] Mäckel H, Varner K, On the determination of the emitter saturation current density from lifetime measurements of silicon devices, Prog Photovoltaics: Res Appl 2012;21:850–866.
[16] Cuevas A, Sinton R, Simple modelling of solar cells, Proceedings 23rd EUPVSEC, Valencia, Spain, 2008. pp. 315–319.
[17] Komatsu Y, Harata D, Schuring EW, Vlooswijk AHG, Shigetaka K, Fujita S, Venema PR, Cesar I, Calibration of electrochemical capacitance-voltage method on pyramid texture surface using scanning electron microscopy 2013;38:94–100.